Acta Crystallographica Section D
Biological Crystallography
ISSN 0907-4449

Structure, modifications and ligand-binding properties of rat profilin 2a

Teemu Haikarainen,[a]‡ Wei-Qiang Chen,[b] Gert Lubec[b] and Petri Kursula[a]*

[a]Department of Biochemistry, University of Oulu, Oulu, Finland, and [b]Department of Pediatrics, Medical University of Vienna, Vienna, Austria

‡ Current address: Turku Centre for Biotechnology, University of Turku and Åbo Akademi, Biocity, Turku, Finland.

Correspondence e-mail: petri.kursula@oulu.fi

Received 26 November 2008
Accepted 7 January 2009

PDB Reference: rat profilin 2a, 2vk3, r2vk3sf.

Profilins are key regulators of the actin microfilament system and in neuronal tissues the profilin 2a isoform is the most abundant and important profilin. The high-resolution crystal structure of rat profilin 2a has been determined in the absence of ligands. By comparing the structure with those of peptide-liganded profilin 2a and unliganded profilin 2b, it can be concluded that the binding site for proline-rich peptides is pre-organized. The C-terminus of profilin 2a is also well ordered in the absence of ligand peptide, in contrast to the 2b isoform which is generated by alternative splicing. Covalent modifications of four cysteine residues were also detected in profilin 2a, as well as a number of other modifications in profilin 2 from rat brain; such modifications could significantly affect the function of profilin. It was also shown that profilin 2a binds to the neuronal protein palladin, including a synthetic palladin peptide; peptides from another profilin ligand, dynamin 1, failed to interact with both profilin 1 and profilin 2a. These results allow a better understanding of the structure–function relationships and ligand binding of mammalian profilin 2a.

1. Introduction

The actin cytoskeleton is responsible for changes in cell shape and motility. Focal contacts, lamellipodia and neuronal growth cone motility all depend on the rapid polymerization and depolymerization of actin. Cells contain several actin-binding proteins that either promote or inhibit actin polymerization.

Profilins are small 15 kDa proteins that bind actin in a stable 1:1 complex. Profilins enhance actin polymerization by adding monomeric globular actin (G-actin) to the growing ends of actin filaments (Kang *et al.*, 1999). They also function as nucleotide-exchange factors, catalysing the exchange of free ATP for actin-bound ADP (Goldschmidt-Clermont *et al.*, 1992). Profilins also bind phosphatidylinositols (Lassing & Lindberg, 1985) and a number of proline-rich ligands (Tanaka & Shibata, 1985; Witke, 2004).

Four mammalian profilins (profilins 1–4) have been found. Profilins 1 and 2 (Pfn1 and Pfn2, respectively) are by far the best characterized mammalian profilins; Pfn2 gives rise to two variants by alternative splicing, which are termed profilins 2a and 2b (Di Nardo *et al.*, 2000; Lambrechts *et al.*, 2000). Of these isoforms, Pfn2a has the higher affinity towards proline-rich ligands (Di Nardo *et al.*, 2000; Lambrechts *et al.*, 2000) and as a consequence of this its interaction with ligand peptides has been intensively studied. Pfn1 is the major form in most

tissues except brain, where Pfn2a is dominant (Honore *et al.*, 1993; Witke *et al.*, 1998). Neuronal Pfn2a is involved in a number of nervous-system processes (Birbach, 2008), such as the regulation of cortical actin; its overexpression results in the suppression of neuritogenesis (Da Silva *et al.*, 2003). The expression of the minor isoform of Pfn2, Pfn2b, is limited to a few tissues (Di Nardo *et al.*, 2000; Lambrechts *et al.*, 2000).

A number of proline-rich ligand proteins have been identified for both Pfn1 and Pfn2a. For Pfn2a, these include a number of proteins that participate in various aspects of nervous-system function (Witke, 2004; Birbach, 2008). Among the ligands of profilin are palladin (Boukhelifa *et al.*, 2006), a protein that interacts with α-actinin (Ronty *et al.*, 2004), and dynamin 1, which is involved in membrane trafficking (Witke *et al.*, 1998; Gareus *et al.*, 2006). Pfn2a-deficient mice show abnormalities in their nervous system and behaviour, including hyperactivity and novelty-seeking behaviour (Pilo Boyl *et al.*, 2007).

The structural data on profilins is extensive (Fedorov *et al.*, 1994; Nodelman *et al.*, 1999) and includes a recent structure of a profilin from the malaria parasite *Plasmodium falciparum* (Kursula, Kursula, Ganter *et al.*, 2008). The crystal structure of human Pfn2b has been determined (Nodelman *et al.*, 1999) and the crystal structures of mouse Pfn2a complexed with ligands from VASP and mDia1 have recently been reported (Kursula, Kursula, Massimi *et al.*, 2008). However, no crystal structure of Pfn2a in the absence of ligand peptides has been published.

Here, we report the crystal structure of unliganded rat Pfn2a. The structure of Pfn2a contains unique features when compared with other published profilin 2 structures: a disulfide bridge between two neighbouring cysteines and two surface cysteines modified by dithiothreitol (DTT). The C-terminal helix, which is partly disordered in the unliganded structure of Pfn2b (Nodelman *et al.*, 1999), is fully ordered in Pfn2a and thus the binding of proline-rich peptides to Pfn2a does not involve large conformational changes. We have further analysed the post-translational modifications in rat profilin 2 using proteomics methods, mapped them onto the three-dimensional structure and characterized the binding of Pfn2a to peptides derived from palladin and dynamin 1.

2. Materials and methods

2.1. Expression, purification and crystallization

Rat Pfn2a was expressed as a GST-fusion protein using the pGEX-4T-2 vector (Loomis *et al.*, 2003). *Escherichia coli* Rosetta (DE3) cells were transformed with the vector and expression was carried out in LB medium supplemented with chloramphenicol (34 µg ml^{-1}) and ampicillin (100 µg ml^{-1}) at 310 K. The culture was grown at 310 K until the OD_{600} was 0.7 and induction was performed with 0.4 m*M* IPTG at 291 K overnight. The cells were harvested and suspended in 50 m*M* HEPES pH 7.5 containing 50 m*M* KCl, 10% glycerol, 1 m*M* DTT, 1 m*M* EDTA and 1% Triton X-100.

Table 1
Data-processing and refinement statistics for rat profilin 2a.

Values in parentheses are for the high-resolution shell.

Data collection	
Resolution range (Å)	20.0–1.70 (1.74–1.70)
Space group	$P4_1$
Unit-cell parameters (Å, °)	$a = b = 51.1$, $c = 67.5$, $\alpha = \beta = \gamma = 90.0$
Completeness (%)	99.0 (99.8)
$R_{\rm merge}$† (%)	6.9 (52.2)
Redundancy	3.1 (3.1)
$\langle I/\sigma(I)\rangle$	12.7 (2.2)
Refinement	
Resolution range (Å)	20.0–1.70
$R_{\rm cryst}$‡ (%)	17.3
$R_{\rm free}$§ (%)	21.6
R.m.s.d. bond lengths (Å)	0.020
R.m.s.d. bond angles (°)	1.8
R.m.s.d. *B* factors of bonded atoms (Å^2)	
Main chain	2.5
Side chain	5.9
Ramachandran plot (%)	
Most favoured	95.4
Additionally allowed	3.9
Not allowed	0.8

† $R_{\rm merge} = \sum_{hkl}\sum_i |I_i(hkl) - \langle I(hkl)\rangle| / \sum_{hkl}\sum_i I_i(hkl)$. ‡ $R_{\rm cryst} = \sum_{hkl} ||F_{\rm obs}| - |F_{\rm calc}|| / \sum_{hkl} |F_{\rm obs}|$. § $R_{\rm free}$ was calculated like $R_{\rm cryst}$ using only a test set of 5% of the data that were not used in refinement.

The cells were disrupted by sonication and the lysate was centrifuged. The supernatant was incubated with glutathione Sepharose 4B (Amersham Pharmacia Biotech) at 277 K for 1 h. The mixture was then applied onto a gravity-flow column and the column was washed with 1× PBS containing 0.1% Triton X-100. The GST-fusion proteins were eluted with 20 m*M* glutathione in 50 m*M* Tris–HCl pH 8.0. The GST tag of the fusion protein was cleaved with 100 U thrombin (Amersham Biosciences) with gentle rotation at room temperature overnight.

Pfn2a was applied onto a Superdex 75 HR 16/60 column (Amersham Biosciences) pre-equilibrated with 50 m*M* Tris–HCl pH 8.0 containing 150 m*M* KCl and elution was carried out in the same buffer. The fractions containing Pfn2a were pooled and concentrated to 10 mg ml^{-1} with Amicon Ultra-15 centrifugal filter devices (Millipore). The protein was shown to be folded, with a melting point of approximately 333 K, by CD spectroscopy and Thermofluor assays (unpublished data).

Pfn2a (in 50 m*M* Tris–HCl pH 8.0, 150 m*M* KCl) was crystallized at 277 K by the sitting-drop vapour-diffusion method using 1 µl protein solution and 1 µl well solution (0.1 *M* acetic acid pH 4.5, 2 *M* ammonium sulfate, 1 *M* NaCl) and equilibrating against 100 µl well solution. The crystals grew to 0.06 mm in size in one month.

2.2. Data collection and structure refinement

Before data collection, a crystal was quickly soaked in well solution supplemented with 10% glycerol as a cryoprotectant. A data set was collected from the crystal on the EMBL BW7A beamline at the DORIS storage ring, DESY, Hamburg. The data were processed, scaled and merged using *XDS* (Kabsch,

1993) and *XDSi* (Kursula, 2004) (Table 1) and 5% of the data were set aside for calculation of the free *R* factor. Molecular replacement was performed with *MOLREP* (Vagin & Teplyakov, 1997) using mouse Pfn2a liganded with a proline-rich domain of VASP (PDB code 2v8c; Kursula, Kursula, Massimi *et al.*, 2008) as a model. Refinement of the structure was performed using *REFMAC*5 (Murshudov *et al.*, 1997) and *phenix.refine* (Adams *et al.*, 2002) and model building was performed in *Coot* (Emsley & Cowtan, 2004).

2.3. Two-dimensional electrophoresis and mass spectrometry

Two-dimensional electrophoresis and mass spectrometry were carried out essentially as previously described (Chen *et al.*, 2006; Majava *et al.*, 2008). A full description of the experimental details can be found as supplementary material.[1]

2.4. Synthetic ligand peptides

The peptides were aquired from GenScript (GenScript Corp., Piscataway, New Jersey, USA). The peptides corresponded to the second proline-rich region of human palladin (FPLPPPPPPLPS, residues 208–219) and the proline-rich regions of mouse dynamin 1 (GGAPPVPSRPGA and PFGPPPQVPSRP, residues 810–821 and 825–836, respectively) suggested to bind Pfn2a with highest affinity (Gareus *et al.*, 2006).

2.5. Pulldown assay

Four different constructs of human palladin (corresponding to residues 8–173, 8–228, 101–301 and 222–387; Boukhelifa *et al.*, 2006) were used to produce GST-fusion proteins that were then bound to glutathione Sepharose. 110 µg Pfn2a was diluted with binding buffer (PBS supplemented with 0.1% Triton X-100 and 1 m*M* DTT) to a final volume of 0.5 ml and added to 25 µl of the matrix with similar amounts of the different GST-palladin fusion proteins bound. The samples were incubated at 277 K for 2 h, after which the Sepharose pellets were consecutively washed four times with 1 ml binding buffer. SDS loading buffer was then added to the Sepharose pellets and the presence of bound Pfn2a was visualized by SDS–PAGE.

2.6. Fluorescence spectroscopy

The binding of poly-L-proline to profilin results in a change in fluorescence (Perelroizen *et al.*, 1994). In profilins, two tryptophans are involved in poly-L-proline binding and therefore an excitation wavelength of 295 nm was used (only tryptophan emission was observed). The measurements were performed with an LS50B luminescence spectrophotometer (Perkin–Elmer instruments, Waltham, Massachusetts, USA). Emission spectra were collected from 300 to 400 nm at 0.5 nm intervals. An integration time of 0.25 s was used. All measurements were performed at a stable temperature of 298 K with a scan speed of 500 nm min^{-1}. The monochromator slit widths were set at 5.0 nm.

The proteins were diluted to 5 µ*M* in 50 m*M* Tris pH 8.0 supplemented with 150 m*M* KCl; this buffer was also used as a blank. The proteins were incubated with the peptides at room temperature for 2 h before measurement. The spectra were integrated between 300 and 315 nm against the blank (containing Pfn2a but no peptide) and the data were fitted using nonlinear least-squares hyperbolae with a one-site binding model.

2.7. Isothermal titration calorimetry

Isothermal titration calorimetry (ITC) measurements were performed at 303 K with a VP-ITC microcalorimeter (MicroCal Inc., Northampton, Massachusetts, USA). 5 µl of 1 m*M* palladin peptide solution was injected 20 times into 0.055 m*M* Pfn2a solution. Buffer was used in control injections to correct for the heat effects that were not directly involved in the binding reaction. These titrations had the same parameters as the measurements, except that 5–10 injections were used.

Both the protein and the peptide were extensively dialysed in the same buffer (100 m*M* potassium phosphate pH 7.6) before measurement and degassed. The data were analysed using *Origin* (MicroCal Software). The measured data were corrected by subtracting the heat of dilution and fitted using the nonlinear least-squares fitting routine.

2.8. Surface plasmon resonance

The binding of the palladin and dynamin 1 peptides to Pfn2a was analysed by surface plasmon resonance (SPR) technology using a Biacore 3000 (Biacore AB, Uppsala, Sweden) instrument. Pfn2a was coupled to a CM5 sensor chip using standard amine-coupling chemistry. The interactions between the peptides and Pfn2a were analysed with peptide concentrations between 50 n*M* and 2 m*M*. 30 µl of the peptide solutions were injected onto the sensor-chip surface at a flow rate of 10 µl min^{-1} at 298 K in the running buffer (10 m*M* HEPES pH 7.4, 150 m*M* NaCl, 3 m*M* EDTA, 0.005% surfactant P20). The observed responses were plotted against peptide concentration and fitted similarly to the fluorescence data above.

3. Results and discussion

3.1. The crystal structure of unliganded rat profilin 2a

The crystal structure of rat Pfn2a was refined at a resolution of 1.70 Å (Table 1), allowing a detailed structural analysis of Pfn2a in the unliganded state. The structure contained 142 amino-acid residues (including a glycine and a serine residue, after thrombin cleavage, at the N-terminus in addition to the full-length sequence of rat Pfn2a), 220 waters, one sulfate ion and two glycerol molecules. Pfn2a has the common profilin-like fold with a central seven-stranded antiparallel β-sheet flanked by C- and N-terminal helices and two short helices (Fig. 1*a*). The similarity of the overall fold of rat Pfn2a to other profilins is indicated by the r.m.s.d. values for the C$^{\alpha}$ positions;

[1] Supplementary material has been deposited in the IUCr electronic archive (Reference: EN5345). Services for accessing this material are described at the back of the journal.

the r.m.s.d.s for rat Pfn2a with mouse liganded Pfn2a (139 aligned C^{α} atoms), human Pfn2b (136 aligned C^{α} atoms), bovine Pfn1 (138 aligned C^{α} atoms), human liganded Pfn1 (138 aligned C^{α} atoms), yeast profilin (121 aligned C^{α} atoms) and *Arabidopsis* profilin (121 aligned C^{α} atoms) are 0.8, 0.8, 0.9, 1.0, 1.9 and 1.8 Å, respectively.

The final electron-density map is of good quality, with the exception of Gly93 and Gly94 in the loop connecting β-strands 5 and 6 for which the density was not complete. Cys25, which is involved in a disulfide bond with DTT (see below), is the only residue in the disallowed region of the Ramachandran plot.

In a number of profilin crystal structures, sulfate or phosphate ions occupy the characterized binding site for phosphatidylinositols, formed, for example, by Arg74, Arg88 and Arg135 (Lambrechts *et al.*, 2002). In the rat Pfn2a structure, the sulfate ion is coordinated by Arg135 and Arg104, thus coinciding with the putative phosphate-binding site for phosphoinositols.

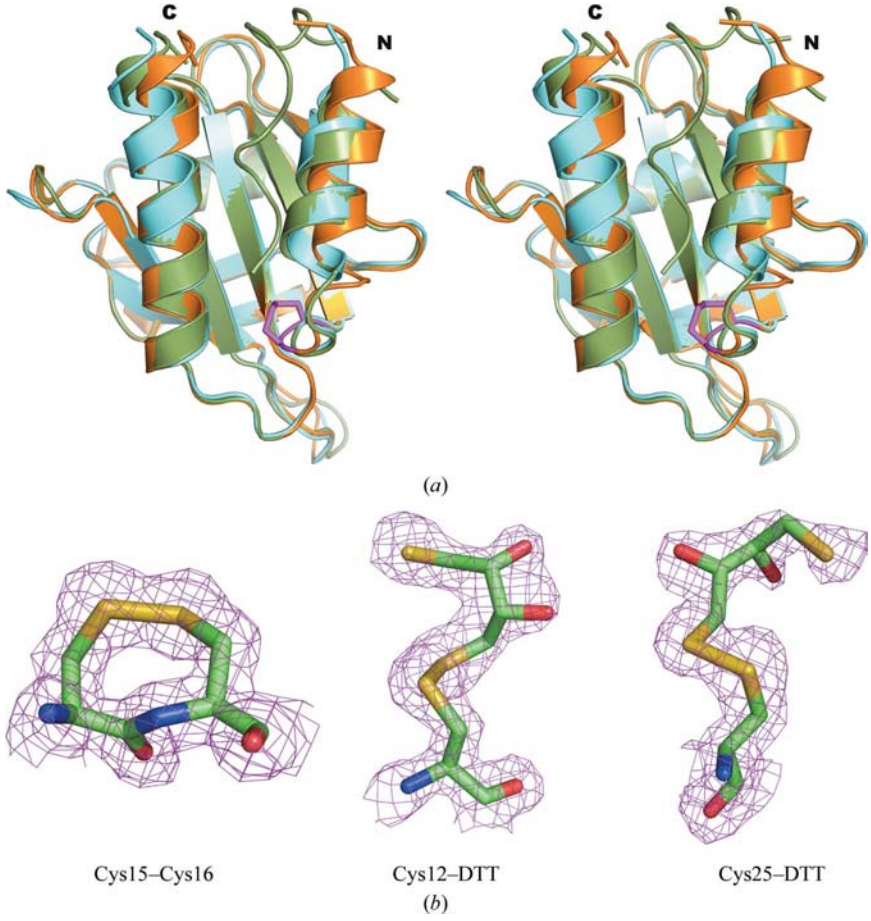

Figure 1
Structural properties of rat Pfn2a. (*a*) The overall structure of rat Pfn2a (orange) and its comparison to those of mouse Pfn2a bound to a ligand peptide from VASP (green) and human unliganded Pfn2b (light blue). Residues 20–120 were used for the superpositioning in order to be able to highlight conformational differences in the N- and C-terminal helices. The disulfide bridge between Cys15 and Cys16 in rat Pfn2a is highlighted in magenta. (*b*) Electron densities for the modified cysteine residues in rat Pfn2a. The electron density is the final refined $2F_o - F_c$ map contoured at 1σ.

3.2. Modification of surface cysteines in the structure

A distinctive difference from other profilin structures published to date is the disulfide bond between cysteines 15 and 16 (Fig. 1*b*). These cysteines are present in all mammalian profilin 2 isoforms, but no disulfide bond has previously been detected. Unusual DTT adducts were additionally found for two surface cysteines, Cys12 and Cys25, of the protein (Fig. 1*b*). There are two further cysteines in the interior of the protein that were not modified by DTT. The formation of adducts with DTT by the two surface cysteines demonstrates their reactivity towards free thiol groups. DTT was only present in the lysis buffer during the very first steps of protein purification. The DTT adducts were therefore most likely to have formed during cell lysis. Since the cells were broken by sonication, it is possible that the heat generated locally by the sonication process promoted the reaction. This observation is of general importance when purifying a protein that may have reactive cysteine residues. It is also noteworthy that Pfn2a crystals were only acquired from one protein batch and that crystals could not be produced from other batches. It is likely that the formation of the thiol adducts in one batch stabilized the crystal lattice; in fact, the adduct at Cys12 is located at the edge of a crystal contact area.

Interestingly, in redox proteomics studies (Fratelli *et al.*, 2002; Vorum *et al.*, 2004), Pfn1 has been characterized as a target for glutathionylation, a modification that links glutathione to a Cys residue *via* a disulfide bridge. The DTT adducts observed in our structure are analogues of this modification and our structure confirms the high reactivity of the surface cysteines of profilin towards covalent modification by sulfhydryl-containing small molecules. Of the four cysteines found to be modified in Pfn2a, only Cys16 is conserved in Pfn1 and no other surface cysteines are present in Pfn1; Cys70 and Cys127 are buried.

Profilins have also previously been shown to undergo oligomer formation, most likely *via* disulfide bridges (Babich *et al.*, 1996; Mittermann *et al.*, 1998; Wopfner *et al.*, 2002; Babich *et al.*, 2005). The reaction can be explained by the presence of reactive cysteine residues on the surface of profilins; in the case of Pfn2a it is clear that all four surface cysteines are reactive and it is possible that oligomers of Pfn2a are formed *via* intermolecular disulfides. In fact, using small-angle X-ray scattering, we observed that the apparent molecular weight and radius of Pfn2a both increase on increasing the protein concentration. The second virial coefficient is thus negative, indicating the presence of attractive interactions between Pfn2a molecules and demonstrating the formation of

oligomeric forms of Pfn2a at high concentrations (unpublished data).

Vicinal disulfide bonds, *i.e.* those formed between cysteine residues that are adjacent in the primary sequence, are generally considered to be 'forbidden' (Wouters *et al.*, 2007), but possible links between redox regulation and vicinal disulfides have been suggested (Carugo *et al.*, 2003; Wouters *et al.*, 2007). In this respect, it is noteworthy to mention that actin is under redox regulation (Lassing *et al.*, 2007). While little evidence, apart from the putative oligomerization mentioned above, at present suggests redox regulation for the function of Pfn2a, such regulation could be possible by covalent modification of surface cysteines.

3.3. Comparison of the structure with that of profilin 2b

The difference between Pfn2a and Pfn2b at the sequence level concerns the C-terminal helix, which closely participates in proline-rich ligand binding *via* its aromatic residues (Tyr133 and Phe139 in Pfn2a). It has been shown that Pfn2a binds to poly-L-proline and proline-rich peptides with high affinity (Petrella *et al.*, 1996; Kursula, Kursula, Massimi *et al.*, 2008). Pfn2b, however, has a significantly lower affinity for poly-L-proline (Di Nardo *et al.*, 2000; Lambrechts *et al.*, 2000). The C-terminal aromatic residue is conserved in Pfn1 (Tyr139) and Pfn2a (Phe139), but in Pfn2b this aromatic residue, which is important for the interactions with proline-rich ligands (Kursula, Kursula, Massimi *et al.*, 2008), is missing. In the crystal structure of human Pfn2b (Nodelman *et al.*, 1999) the C-terminal helix was somewhat disordered and the C-terminus was not visible; because of this, it was not certain whether or not the C-terminus of Pfn2a was ordered in the absence of ligand peptides. Our structure clearly indicates that the C-terminal helix is well defined all the way to the terminal COOH group (Fig. 2*a*), which is anchored inside Pfn2a *via* interactions with the backbone N atoms of Gly106 and Arg107, which are located in a tight turn between β-strands 6 and 7. In fact, it should also be noted that the exact length of the C-terminus in Pfn2b, which is fixed in Pfn1 and Pfn2a, is not absolutely conserved even in closely related species; this implies that there has been no evolutionary pressure to conserve the C-terminus of Pfn2b and this is linked to the poor (if any) interaction of Pfn2b with proline-rich ligands.

In line with the observation that Pfn2a and Pfn2b have similar affinities towards actin (Lambrechts *et al.*, 2000), the actin-binding surfaces of the two proteins are practically identical (Fig. 2*b*). On the other hand, Pfn2b has a weaker affinity towards phosphoinositols than Pfn2a or Pfn1 (Lambrechts *et al.*, 2000), which may be caused by the absence of Arg135, a residue that is commonly seen to bind sulfate ions in profilin crystal structures, in Pfn2b. Both Arg135 and Arg136 were found to be important in Pfn1 for binding (Lambrechts *et al.*, 2002).

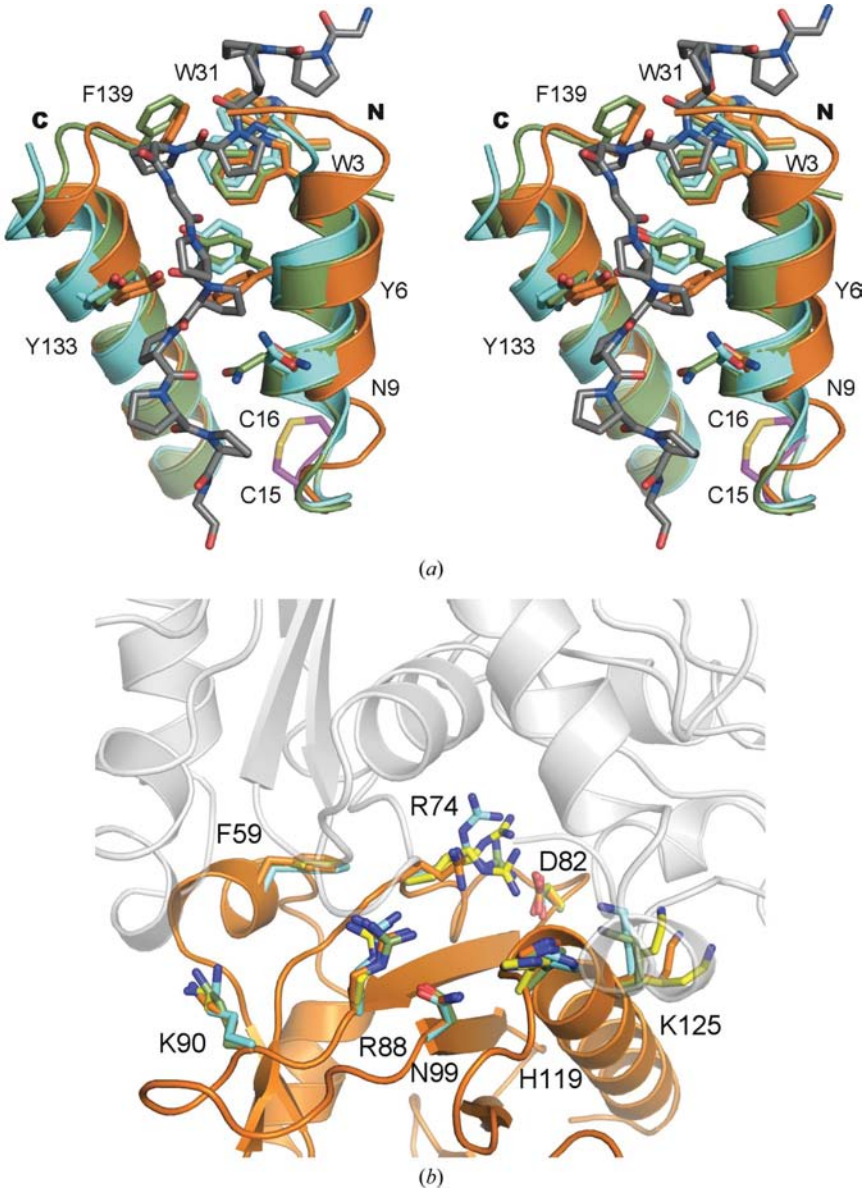

Figure 2
Detailed comparisons between rat Pfn2a and previous structures of Pfn2. (*a*) The proline-rich peptide-binding site. Colouring as in Fig. 1(*a*), except that the VASP peptide is in grey. Note that the C-terminus of Pfn2b is disordered, while the terminal Phe139 is well defined in Pfn2a both in the presence and absence of peptide ligand. (*b*) The actin-binding site. For clarity, the backbone is only shown for rat Pfn2a (orange). The side chains of key actin-binding residues are shown from rat Pfn2a, human Pfn2b (light blue) and mouse Pfn2a in complex with ligand peptides from VASP (green) and mDia1 (yellow). A ghost of bound actin is also shown from the complex between actin and Pfn1 (Ferron *et al.*, 2007). Note the different conformations of Arg74, a central actin-interacting residue, in the various structures.

3.4. Comparison to peptide complexes

In our previous study on ligand peptide binding by mouse Pfn2a at high resolution, we could visualize the fine details of peptide–profilin interactions. Depending on the peptide, three or four direct hydrogen bonds were formed between profilin side chains and the peptide backbone carbonyl O atoms; in addition, CH–π bonds existed between CH groups from the peptide and all individual aromatic rings in the binding site (Kursula, Kursula, Massimi *et al.*, 2008). The central Pfn2a residues that interact with the peptides include Trp3, Tyr6, Asn9, Trp31, Tyr133 and the C-terminal Phe139. A comparison of the binding surface (Fig. 2*a*) indicates that the side-chain rotamer conformations of Tyr6 and Asn9 differ between the liganded and unliganded structures; the same is true for Met130 (not shown), which is engaged in a van der Waals interaction with the peptide in the complexes. Small changes are also seen in the conformations of Tyr133 and Phe139, while the two tryptophans in the binding site remain unaltered.

The binding site for proline-rich ligands in profilins is preorganized. The current structure supports this view, despite the fact that the N-terminal helix has shifted away slightly from the C-terminal helix (Fig. 2*a*) and the side-chain conformations of Tyr6 and Asn9 are different from the liganded structures. It is likely that the disulfide between Cys15 and Cys16 forces this shift of the N-terminal helix and the previously unobserved side-chain conformation of Tyr6. In fact, in molecular-dynamics simulations we have observed that removal of the disulfide bond eventually causes the N-terminal helix to return to its 'normal' position (unpublished data). Importantly, the C-terminal helix is also fully ordered in Pfn2a in the absence of peptide ligand.

3.5. The detection of two isoforms of profilin 2 in rat hippocampus using two-dimensional electrophoresis and mass spectrometry

When identifying all the spots in rat hippocampus two-dimensional gels in our previous study (Chen *et al.*, 2006), two spots were identified as Pfn2 (Fig. 3*a*). In order to shed light on the post-translational modifications (PTMs) present in Pfn2, these two spots were picked, digested with trypsin and chymotrypsin and analysed by nano-LC-ESI-CID/ETD-MS/MS. The results are summarized in supplementary Table 1. It is noteworthy that deamidation of Asn61 and Gln92, as well as oxidation of Met86, were detected in both spots. We also detected deamidation of Gln17 in spot 1. In spot 2, we observed acetylation of Ala1, deamidation of Asn9, Gln40 and Asn99, deimidation of Arg74 and Arg88, methylation of Glu95 (possibly caused by methanol during staining, based on our previous experience) and oxidation of Met11 and Met113.

The difference in the observed isoelectric point of the two spots strongly suggests that the spots represent the two alternatively spliced isoforms profilin 2a and 2b. This is further indicated by the fact that for spot 2 sequences covering the C-terminus specific to Pfn2a were detected using both trypsin and chymotrypsin, but for spot 1 no C-terminal peptide after the splice site at residue 107 was detected. The observed pIs for the two spots also closely match those calculated for the two splice isoforms. While Pfn2a is clearly the predominant profilin isoform in the brain, low levels of Pfn2b expression have also been detected (Di Nardo *et al.*, 2000).

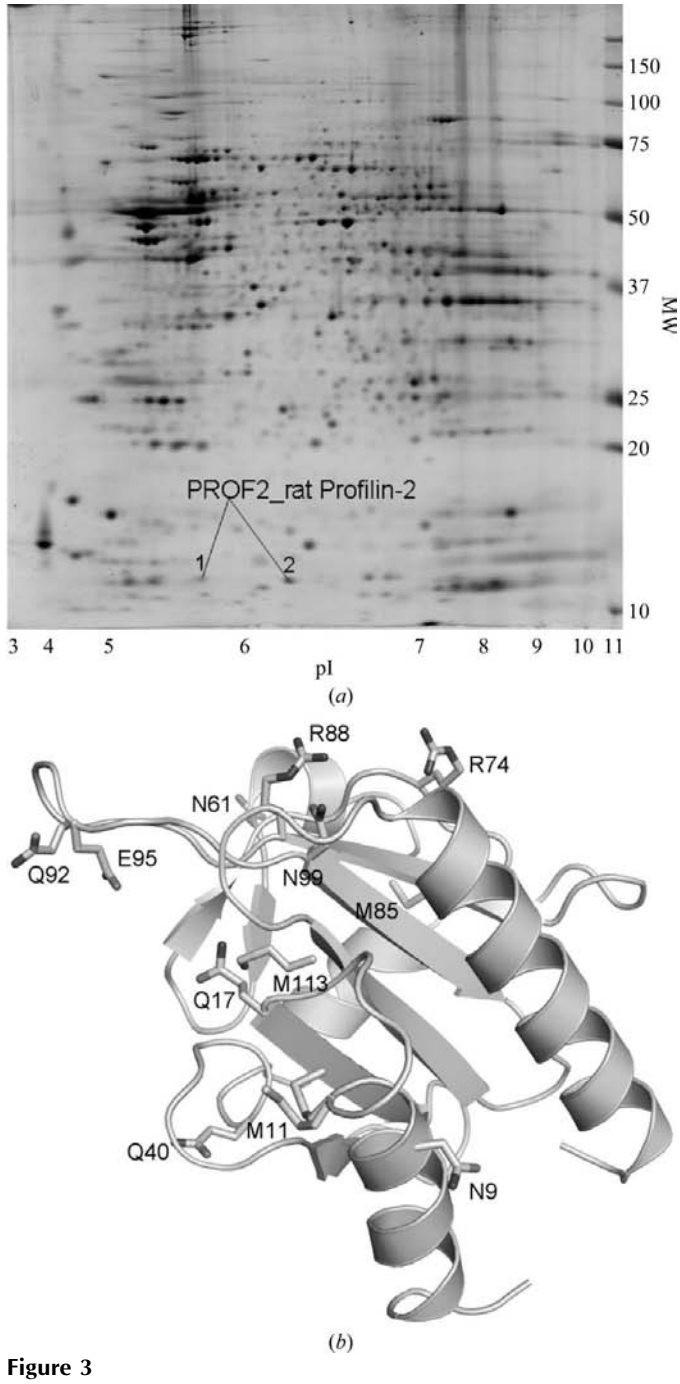

Figure 3
Two-dimensional electrophoresis and mapping of post-translational modifications. (*a*) Two-dimensional electrophoresis gel of rat brain hippocampus, with spots identified as Pfn2 highlighted. The details of the selected spots are given in supplementary Table 1. The molecular-weight standards (kDa) are indicated on the right and the pI values at the bottom. (*b*) Mapping of the detected modified residues onto the crystal structure of Pfn2a. The view is such that the actin-binding surface is at the top and the proline-rich ligand-binding site at the bottom right, between the N- and C-terminal helices.

The PTMs are located on the surface of Pfn2 and many of the modifications may thus have functional consequences. For example, deamidation is a spontaneously occurring modification of Asn and Gln residues that is commonly detected upon aging (Lindner & Helliger, 2001). Of the modified residues, Asn9 is located at the binding site for proline-rich ligands, while the residues Arg74, Arg88 and Asn99 are centrally located on the actin-binding surface and are known to be important for actin binding. The deimidation (citrullination) of Arg74 and Arg88 could be the result of enzymatic action by peptidylarginine deiminase (Gyorgy *et al.*, 2006). These results suggest that during aging Pfn2a accumulates PTMs in the brain; this may adversely affect its function as a regulator of the actin cytoskeleton.

3.6. Binding of profilin 2a to palladin and dynamin 1

Since Pfn2a is mainly a neuronal profilin isoform, we analysed the binding of rat Pfn2a to synthetic peptides taken from two nervous-system ligands: palladin and dynamin 1. Firstly, the binding of Pfn2a to various GST-tagged constructs of palladin was analysed (Fig. 4*a*) and the results indicated its interaction with the constructs containing proline-rich segments, most strongly with that containing only the second proline-rich domain (residues 101–301). The results are similar to those observed previously using Pfn1 (Boukhelifa *et al.*, 2006).

The binding of Pfn2a to a peptide from the second proline-rich region of human palladin (Boukhelifa *et al.*, 2006), as well as to two peptides from dynamin 1 that were characterized as binding sites for mouse Pfn2a (Gareus *et al.*, 2006), was studied by ITC, fluorescence spectroscopy and SPR. In the fluorescence spectroscopy experiment rat Pfn1 was also studied. The results of the fluorescence titration clearly indicated that while both Pfn1 and Pfn2a bound the palladin peptide (Fig. 4*b*), very low affinity, if any, could be detected towards either of the peptides from dynamin 1. A low affinity in the millimolar range could be seen for the peptide closer to the C-terminus of dynamin 1. The result is somewhat surprising, since the two dynamin peptides were exactly those that had been shown to bind Pfn2a most strongly in a previous ligand-blotting experiment (Gareus *et al.*, 2006). Furthermore, in a pulldown

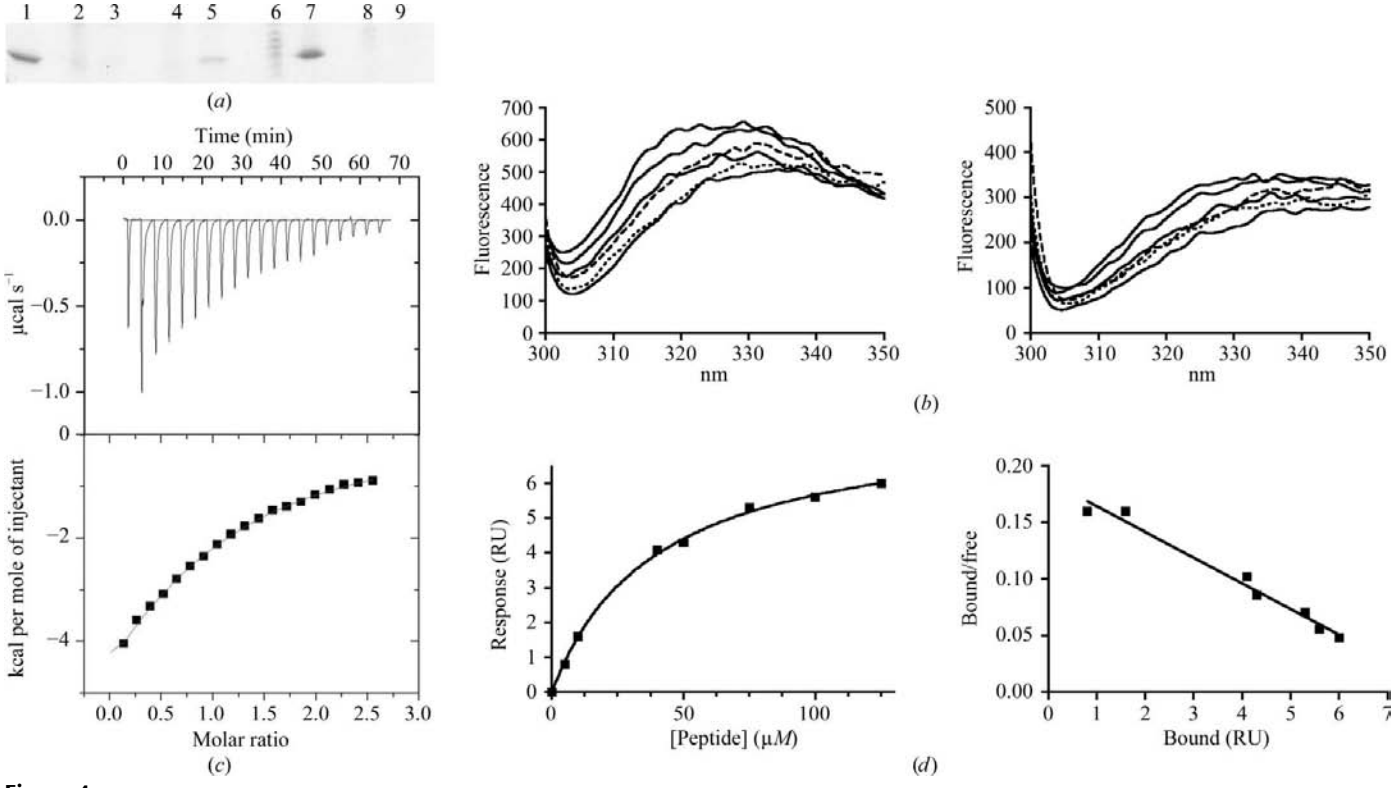

Figure 4

Binding of rat Pfn2a to palladin and dynamin 1. (*a*) Pulldown assay of purified Pfn2a on glutathione Sepharose-bound GST-fusion proteins of palladin. The samples are as follows: 1, Pfn2a control; 2 and 3, GST-palladin(8–173) before and after incubation with Pfn2a; 4 and 5, GST-palladin(8–228) before and after incubation with Pfn2a; 6 and 7, GST-palladin(101–301) before and after incubation with Pfn2a; 8 and 9, GST-palladin(222–387) before and after incubation with Pfn2a. (*b*) Fluorescence spectroscopy. Shown are selected raw curves from the concentration series. Left, Pfn2a; right, Pfn1. In both graphs the four solid lines represent concentrations of 0, 25, 50 and 100 µ*M* of the palladin peptide (from bottom to top, respectively), the dashed line represents 1.5 m*M* dynamin 1 peptide PFGPPPQVPSRP and the dotted line represents 1.5 m*M* dynamin 1 peptide GGAPPVPSRPGA. (*c*) ITC analysis of binding between Pfn2a and the palladin peptide. The top part shows the raw baseline-corrected titration curve, while the bottom graph shows the results of peak integration. (*d*) SPR analysis of binding between Pfn2a and the palladin peptide; left, binding curve; right, Scratchard plot. The low response levels indicate that the majority of immobilized Pfn2a is not competent for binding peptide ligands. Very high concentrations of the dynamin peptide are required for a detectable response (not shown).

Table 2
Binding parameters for the interaction between Pfn2a and ligand peptides using different methods.

n.d., not tested.

	Palladin peptide FPLPPPPPPLPS	Dynamin 1 peptide GGAPPVPSRPGA	Dynamin 1 peptide PFGPPPQVPSRP
Fluorescence spectroscopy			
K_d (μM)	48 ± 9 (Pfn1), 71 ± 12 (Pfn2a)	No binding	>500 (Pfn1), >500 (Pfn2a)
Surface plasmon resonance			
K_d (μM)	39 ± 3	n.d.	>1000
Isothermal titration calorimetry			
K_d (μM)	76 ± 5	n.d.	n.d.
ΔH (kJ mol^{-1})	−51.1 ± 5.0	n.d.	n.d.
$-T\Delta S$ (kJ mol^{-1})	27.2	n.d.	n.d.
ΔG (kJ mol^{-1})	−23.9	n.d.	n.d.
n	0.73 ± 0.06	n.d.	n.d.

assay, it has been shown that Pfn2a bound recombinant dynamin 1 much more strongly than Pfn1 (Gareus *et al.*, 2006). An explanation for the lack of interaction here may be the lack of five consecutive proline residues in the peptides and the fact that the peptides were free in solution, instead of being immobilized. In a previous study, we showed using a panel of peptides from mDia1, including a number of mutated ones, that a stretch of a minimum of five proline residues was required for binding to mouse Pfn2a (Kursula, Kursula, Massimi *et al.*, 2008).

Binding of the palladin peptide to Pfn2a was also confirmed by ITC (Fig. 4*c*) and SPR (Fig. 4*d*) and the affinity was in the range 39–79 μM in all experiments. Such affinity is normal for a profilin–peptide complex and is also seen for mouse Pfn2a towards peptides from VASP and mDia1 (Kursula, Kursula, Massimi *et al.*, 2008). The energetics of the interaction also very closely resemble those seen for the latter peptide ligands when binding to mouse Pfn2a, suggesting a similar mode of interaction. The results of the peptide-binding assays are collected in Table 2.

4. Conclusions

We have presented the first crystal structure of the mammalian neuronal profilin isoform Pfn2a in the absence of ligand peptides. The structure proves that no large-scale conformational changes accompany proline-rich ligand binding in Pfn2a and that, unlike Pfn2b (Nodelman *et al.*, 1999), the C-terminus of Pfn2a is also well ordered in the absence of a ligand peptide. The reactivity of the surface cysteines, as well as the detected PTMs in brain Pfn2, suggest that the function of Pfn2a in the brain can be regulated by a number of modifications. We also showed that like Pfn1 (Boukhelifa *et al.*, 2006), Pfn2a also interacts with palladin *in vitro* and that the peptides from dynamin 1, previously suggested to be Pfn2a ligands (Gareus *et al.*, 2006), failed to interact with both Pfn1 and Pfn2a with high affinity. Together, our results provide a structural framework for better understanding the structure–function relationships in Pfn2a and the factors that may affect the function of this important regulator of microfilaments.

We wish to thank Dr James Bartles for providing the Pfn2a expression clone and Professor Olli Carpén for the palladin expression constructs. We also thank Dr Inari Kursula for helpful discussions and comments and Viivi Majava for careful supervision in the laboratory. The beamline support at EMBL Hamburg is gratefully acknowledged. This study was supported by grants from the Academy of Finland (PK) and the Department of Biochemistry, University of Oulu (TH). Crystallographic data collection at EMBL Hamburg was supported by the European Community Research Infrastructure Action under the FP6 'Structuring the European Research Area' Programme (through the Integrated Infrastructure Initiative 'Integrating Activity on Synchrotron and Free Electron Laser Science'), contract RII3-CT-2004-506008(IA-SFS).

References

Adams, P. D., Grosse-Kunstleve, R. W., Hung, L.-W., Ioerger, T. R., McCoy, A. J., Moriarty, N. W., Read, R. J., Sacchettini, J. C., Sauter, N. K. & Terwilliger, T. C. (2002). *Acta Cryst.* D**58**, 1948–1954.
Babich, M., Foti, L. R., Sykaluk, L. L. & Clark, C. R. (1996). *Biochem. Biophys. Res. Commun.* **218**, 125–131.
Babich, M., Foti, L. R., Wong, L. & Pack, G. R. (2005). *Proc. West. Pharmacol. Soc.* **48**, 39–43.
Birbach, A. (2008). *Bioessays*, **30**, 994–1002.
Boukhelifa, M., Moza, M., Johansson, T., Rachlin, A., Parast, M., Huttelmaier, S., Roy, P., Jockusch, B. M., Carpen, O., Karlsson, R. & Otey, C. A. (2006). *FEBS J.* **273**, 26–33.
Carugo, O., Cemazar, M., Zahariev, S., Hudaky, I., Gaspari, Z., Perczel, A. & Pongor, S. (2003). *Protein Eng.* **16**, 637–639.
Chen, W. Q., Kang, S. U. & Lubec, G. (2006). *Nature Protoc.* **1**, 1446–1452.
Da Silva, J. S., Medina, M., Zuliani, C., Di Nardo, A., Witke, W. & Dotti, C. G. (2003). *J. Cell Biol.* **162**, 1267–1279.
Di Nardo, A., Gareus, R., Kwiatkowski, D. & Witke, W. (2000). *J. Cell Sci.* **113**, 3795–3803.
Emsley, P. & Cowtan, K. (2004). *Acta Cryst.* D**60**, 2126–2132.
Fedorov, A. A., Magnus, K. A., Graupe, M. H., Lattman, E. E., Pollard, T. D. & Almo, S. C. (1994). *Proc. Natl Acad. Sci. USA*, **91**, 8636–8640.
Ferron, F., Rebowski, G., Lee, S. H. & Dominguez, R. (2007). *EMBO J.* **26**, 4597–4606.
Fratelli, M., Demol, H., Puype, M., Casagrande, S., Eberini, I., Salmona, M., Bonetto, V., Mengozzi, M., Duffieux, F., Miclet, E., Bachi, A., Vandekerckhove, J., Gianazza, E. & Ghezzi, P. (2002). *Proc. Natl Acad. Sci. USA*, **99**, 3505–3510.
Gareus, R., Di Nardo, A., Rybin, V. & Witke, W. (2006). *J. Biol. Chem.* **281**, 2803–2811.
Goldschmidt-Clermont, P. J., Furman, M. I., Wachsstock, D., Safer, D., Nachmias, V. T. & Pollard, T. D. (1992). *Mol. Biol. Cell*, **3**, 1015–1024.
Gyorgy, B., Toth, E., Tarcsa, E., Falus, A. & Buzas, E. I. (2006). *Int. J. Biochem. Cell Biol.* **38**, 1662–1677.
Honore, B., Madsen, P., Andersen, A. H. & Leffers, H. (1993). *FEBS Lett.* **330**, 151–155.
Kabsch, W. (1993). *J. Appl. Cryst.* **26**, 795–800.

Kang, F., Purich, D. L. & Southwick, F. S. (1999). *J. Biol. Chem.* **274**, 36963–36972.
Kursula, I., Kursula, P., Ganter, M., Panjikar, S., Matuschewski, K. & Schüler, H. (2008). *Structure*, **16**, 1638–1648.
Kursula, P. (2004). *J. Appl. Cryst.* **37**, 347–348.
Kursula, P., Kursula, I., Massimi, M., Song, Y. H., Downer, J., Stanley, W. A., Witke, W. & Wilmanns, M. (2008). *J. Mol. Biol.* **375**, 270–290.
Lambrechts, A., Braun, A., Jonckheere, V., Aszodi, A., Lanier, L. M., Robbens, J., Van Colen, I., Vandekerckhove, J., Fassler, R. & Ampe, C. (2000). *Mol. Cell. Biol.* **20**, 8209–8219.
Lambrechts, A., Jonckheere, V., Dewitte, D., Vandekerckhove, J. & Ampe, C. (2002). *BMC Biochem.* **3**, 12.
Lassing, I. & Lindberg, U. (1985). *Nature (London)*, **314**, 472–474.
Lassing, I., Schmitzberger, F., Bjornstedt, M., Holmgren, A., Nordlund, P., Schutt, C. E. & Lindberg, U. (2007). *J. Mol. Biol.* **370**, 331–348.
Lindner, H. & Helliger, W. (2001). *Exp. Gerontol.* **36**, 1551–1563.
Loomis, P. A., Zheng, L., Sekerkova, G., Changyaleket, B., Mugnaini, E. & Bartles, J. R. (2003). *J. Cell Biol.* **163**, 1045–1055.
Majava, V., Loytynoja, N., Chen, W. Q., Lubec, G. & Kursula, P. (2008). *FEBS J.* **275**, 4583–4596.
Mittermann, I., Fetrow, J. S., Schaak, D. L., Almo, S. C., Kraft, D., Heberle-Bors, E. & Valenta, R. (1998). *Sex. Plant Reprod.* **11**, 183–191.
Murshudov, G. N., Vagin, A. A. & Dodson, E. J. (1997). *Acta Cryst.* D**53**, 240–255.
Nodelman, I. M., Bowman, G. D., Lindberg, U. & Schutt, C. E. (1999). *J. Mol. Biol.* **294**, 1271–1285.
Perelroizen, I., Marchand, J. B., Blanchoin, L., Didry, D. & Carlier, M. F. (1994). *Biochemistry*, **33**, 8472–8478.
Petrella, E. C., Machesky, L. M., Kaiser, D. A. & Pollard, T. D. (1996). *Biochemistry*, **35**, 16535–16543.
Pilo Boyl, P., Di Nardo, A., Mulle, C., Sassoe-Pognetto, M., Panzanelli, P., Mele, A., Kneussel, M., Costantini, V., Perlas, E., Massimi, M., Vara, H., Giustetto, M. & Witke, W. (2007). *EMBO J.* **26**, 2991–3002.
Ronty, M., Taivainen, A., Moza, M., Otey, C. A. & Carpen, O. (2004). *FEBS Lett.* **566**, 30–34.
Tanaka, M. & Shibata, H. (1985). *Eur. J. Biochem.* **151**, 291–297.
Vagin, A. & Teplyakov, A. (1997). *J. Appl. Cryst.* **30**, 1022–1025.
Vorum, H., Ostergaard, M., Hensechke, P., Enghild, J. J., Riazati, M. & Rice, G. E. (2004). *Proteomics*, **4**, 861–867.
Witke, W. (2004). *Trends Cell Biol.* **14**, 461–469.
Witke, W., Podtelejnikov, A. V., Di Nardo, A., Sutherland, J. D., Gurniak, C. B., Dotti, C. & Mann, M. (1998). *EMBO J.* **17**, 967–976.
Wopfner, N., Willeroidee, M., Hebenstreit, D., van Ree, R., Aalbers, M., Briza, P., Thalhamer, J., Ebner, C., Richter, K. & Ferreira, F. (2002). *Biol. Chem.* **383**, 1779–1789.
Wouters, M. A., George, R. A. & Haworth, N. L. (2007). *Curr. Protein Pept. Sci.* **8**, 484–495.